Journal of Materials Chemistry A

Accepted Manuscript

ROYAL SOCIETY OF CHEMISTRY

www.rsc.org/materialsA

Journal Name

ARTICLE

Molecular Engineering of Benzothienoisoindigo Copolymers Allowing Highly Preferential Face-on Orientations

Received 00th January 20xx,
Accepted 00th January 20xx

DOI: 10.1039/x0xx00000x

www.rsc.org/

Marina Ide[a], Akinori Saeki*[a], Yoshiko Koizumi[a], Tomoyuki Koganezawa[b] and Shu Seki*[a,c]

Orientation of conjugated polymer is increasingly important in organic photovoltaics (OPV) to achieve high power conversion efficiency (PCE). The optimized orientation of conjugated backbones for photo-generated charge carriers in OPV is contrasting to the organic semiconductor devices, demanding new strategies to control and realize face–on orientation of the conjugated systems onto the substrates. Here we report new conjugated polymers composed of electron-accepting benzothienoisoindigo (BTIDG), an asymmetric unit of isoindigo and thienoisoindigo. BTIDG was coupled with weakly-electron-donating thiazolothiazole or benzobisthiazole, concurrently leading to the moderate optical bandgaps (1.41–1.52 eV) and the highest occupied molecular orbital (-5.35– -5.50 eV). Alkythiophene spacer between BTIDG and donor unit provided a marked control over the orientation of polymers, among which the degree of face-on orientation as high as 95 % was revealed by grazing incidence X-ray diffraction. The maximum PCE was improved up to 4.2 % using the system with [6,6]-Phenyl-C_{71}-butyric acid methyl ester ($PC_{71}BM$). We present a useful basis on structure (orientation)-property (OPV output) relationship to lay down new guidelines for the design of efficient solar cell material.

Introduction

A low bandgap polymer (LBP) constituted of electron donor and acceptor units is expected to create an efficient organic photovoltaic (OPV),[1-4] due to its wide photoabsorption and the deep highest occupied molecular orbital (HOMO). Thienoisoindigo (TIDG), analogous to isoindigo (IDG)[5-7] is a comparatively new electron acceptor which we[8] and other groups[9,10] have reported in 2012–2013. Replacing phenyl of IDG by thiophene led to a more planar π-plane and stronger electron accepting ability than IDG. However, TIDG resulted in excessively-narrow optical bandgap (E_g^{opt}, 1.0–1.1 eV) in conjugation with the benchmark donors (benzodithiophene and cychlopentadithiophene).[8] The unsatisfactory PCE of 1.4 % was obtained as the best value in the blend of [6,6]-Phenyl-C_{61}-butyric acid methyl ester ($PC_{61}BM$) and fluorene-TIDG polymer (E_g^{opt} = 1.6 eV).[11] In addition to their mismatches in energy alignment, we have identified the limiting factors of photovoltaic performance, i.e. the short exciton lifetime, the loss via bulk charge recombination, and unfavorable orientation/morphology partly associated with insufficient solubility.[11] Therefore, simultaneous control of these factors through molecular engineering or processing is a crucial prerequisite towards boosting PCE of TIDG-based polymer; however this is a challenging theme shared by all disciplines.

One of the synthetic routes of TIDG unit we have reported for the first time is the dimerization of mono-keto and di-keto precursors in acetic acid, the former of which was prepared by reacting the di-keto precursor with hydrazine reagent followed by Wolff-Kishner type reduction.[8] Inspired from this quantitative and heterotic dimerization scheme, we attempted synthesis of half-TIDG and half-IDG unit from their relevant two precursors. This would bring moderate electron accepting nature with a good solubility as a result of its asymmetric half-distorted π-plane. In the course of the research, Chen and Fréchet *et al.*[12] reported this benzothienoisoindigo (BTIDG)-based polymers synthesized by the almost similar route and demonstrated the large improvement of PCE (4.7%) in terthiophene-BTIDG copolymer. Notably, they realized selective manipulation of edge-on or face-on orientation of polymer by controlling the backbone planarity (IDG or BTIDG) suitable for field-effect transistor (FET) or OPV, respectively. However, the high-performing BTIDG copolymer still includes some portions of edge-on contribution, suggestive of an extra room for enhancing the portion of face-on orientated polymer crystallite where considerable improvement has been reported in both charge carrier transport and overall PCE of OPV devices.[13]

In this work, we synthesized novel BTIDG-based copolymers in combination with benzobisthiazole (BBTz)[14,15] or thiazolothiazole (TzTz),[16,17] where BBTz and TzTz are normally electron acceptors but used as weak donors[18-20]

[a] Department of Applied Chemistry, Graduate School of Engineering, Osaka University, 2-1 Yamadaoka, Suita, Osaka 565-0871, Japan.
[b] Japan Synchrotron Radiation Research Institute, 1-1-1, Kouto, Sayo-cho, Sayo-gun, Hyogo 679-5198, Japan.
[c] Department of Molecular Engineering, Graduate School of Engineering, Kyoto University, Nishikyo-ku, Kyoto 615-8510, Japan.
E-mail: saeki@chem.eng.osaka-u.ac.jp, seki@moleng.kyoto-u.ac.jp

†Electronic Supplementary Information (ESI) available: Details of monomer synthesis and Fig. S1-S7. For ESI see DOI: 10.1039/x0xx00000x

Table 1. Optical and Electrochemical Properties of BTIDG Polymers.

Polymer	M_w / kg mol^{-1} (PDI)	HOMO /eV [a]	LUMO /eV [b]	λ_{max} /nm[c]	E_g^{opt} / eV [d]
TT1	32 (1.7)	-5.35	-3.94	718	1.41
TT2	127 (3.5)	-5.43	-3.98	719	1.45
BT1	142 (2.1)	-5.50	-3.98	690	1.52
BT2	231 (3.9)	-5.41	-3.92	699	1.49

[a] Determined by PYS of drop-casted films. [b] HOMO + E_g^{opt}. [c] In film states. [d] Determined from onset of the electronic absorption spectra in film states.

against BTIDG. This molecular design is intended to provide both optimal E_g^{opt} (ideally 1.37–1.45 eV from the calculation)[21] and HOMO level. Furthermore, we exemplified the synergetic impact of alkylthiophene spacer on the control of polymer orientation and OPV output.

Results and discussion

Optical and Electrochemical Properties.

The brominated BTIDG monomer (9) and alkylthiophene-BTIDG monomer (11) were synthesized according to the route of Scheme 1. Synthesis and characterization of the compounds (1)-(8) including ^{1}H NMR and mass spectroscopy data are provided in Schemes S1. The BTDTG-based copolymers were polymerized by Stille coupling reaction (Scheme 2).

Fig. 1a shows the chemical structures of BTIDG-based copolymers: **TT1**, **TT2**, **BT1**, and **BT2**, in which the number (1 or 2) represents the length of alkylthiophene spacer (thiophene or bithiophene). Electronic absorption spectra of BTIDG polymers were measured in chloroform solution (Fig.

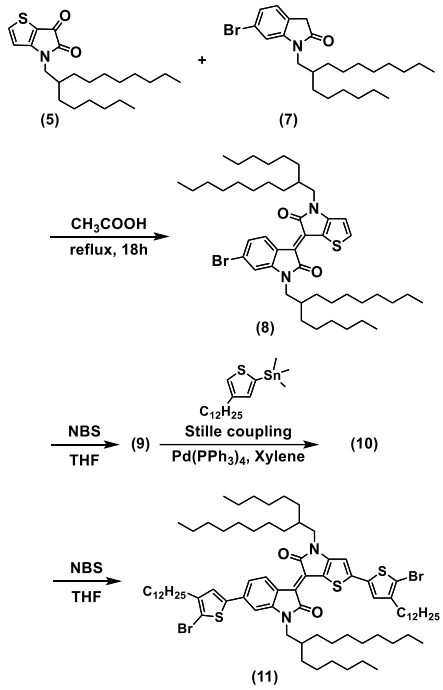

Scheme 1. Synthetic procedure of BTIDG unit. Those of (5) and (7) are provided in Supporting Information.

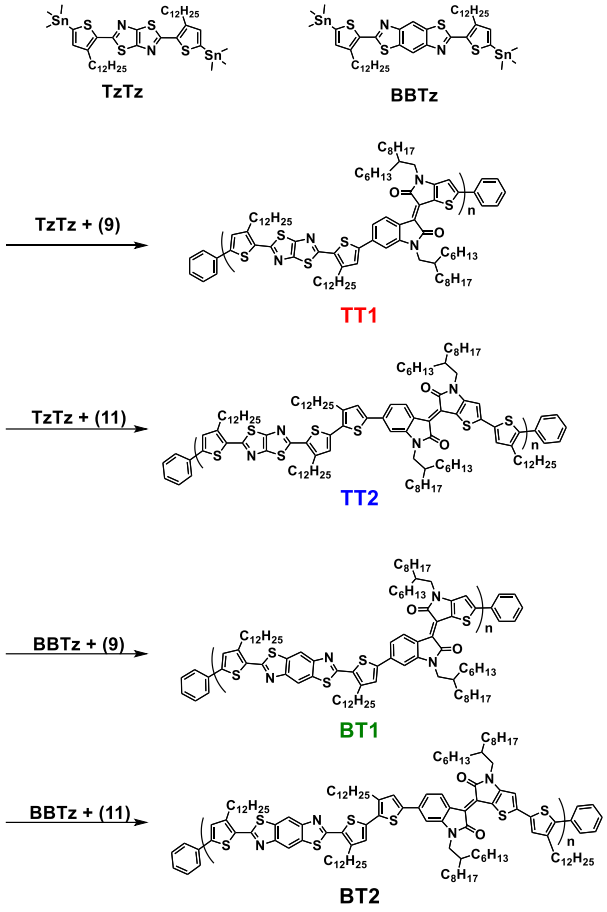

Scheme 2. Synthesis of BTIDG polymers.

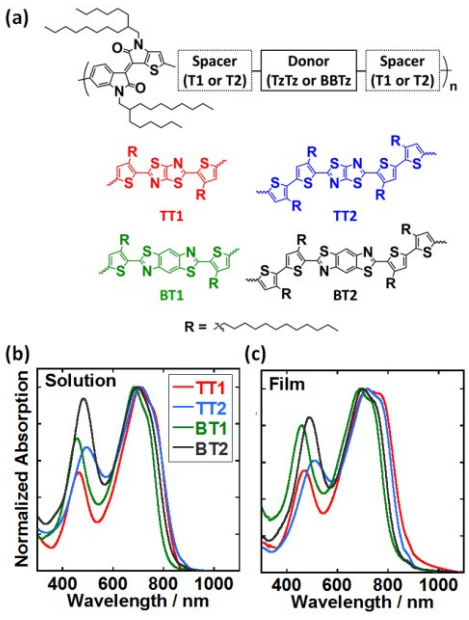

Fig. 1. (a) Chemical structures of BTIDG polymers. (b) Electronic absorption spectra of **TT1** (red line), **TT2** (blue line), **BT1** (green line) and **BT2** (black line) in chloroform solution at room temperature, respectively. (c) Electronic absorption spectra of **TT1**, **TT2**, **BT1** and **BT2** as films dropcast from chloroform solution.

1b) and thin film (Fig. 1c). The BTIDG polymers indicate the absorption edges at ca. 820–880 nm corresponding to the E_g^{opt} of 1.41–1.52 eV (Table 1). These E_g^{opt} are finely tuned to the aforementioned ideal value for single cell OPV polymer,[21] which is a notable advantage over the previous near-infrared absorbing TIDG polymers. In addition, the weight-averaged molecular weights (M_w) of BTIDG polymers are as high as 127–231 kg mol^{-1} (Table 1) except for **TT1** (32 kg mol^{-1}), which is much higher than the previous TIDG polymers (15–87 kg mol^{-1}).[8] This is because that the solubility was significantly improved by virtue of the long linear alkyl chains of thiophene spacer and branched ones of asymmetric BTIDG.

Photoelectron yield spectroscopy (PYS, Fig. S1) was performed to estimate the HOMO levels of polymer films, giving almost identical HOMO (-5.35– -5.50 eV) and slightly-varying the lowest unoccupied molecular orbital (LUMO, -3.92– -3.98 eV). These HOMOs are indeed much deeper than those of our previous TIDG polymers (HOMO: -4.7– -5.4 eV, LUMO: -3.8 eV),[8] while the LUMO-LUMO offsets between polymer and PCBM (-4.2 eV)[22] became close to or even less than the empirically-required minimum value (0.3 eV).[23,24]

Electron withdrawing nature of BTIDG unit is clearly evident from the density functional theory (DFT) calculation shown in Fig. S2. The LUMO is localized on the BTIDG unit, while the HOMO is spread over the polymer backbone of donor (BT or TT), spacer (thiophene), and BTIDG, similar to the TIDG[8] and IDG[25] polymers. Thanks to the inherently high coplanarity and low LUMO, TIDG-thiophene and -naphthalene copolymers have uncovered ambipolar charge transport (μ_h = 0.18 cm^{2}V^{-1}s^{-1} and μ_e = 0.03 cm^{2}V^{-1}s^{-1})[26] and ultrahigh hole mobility up to 14 cm^{2}V^{-1}s^{-1},[27] respectively. In addition, nonbonding Coulomb interaction arisen from the difference in electronegativity of sulfur atom of spacer thiophene and nitrogen atom of TT and BT could facilitate coplanarity of π-conjugated polymer backbone. This is supported by DFT calculation exhibiting that the total energy of N…S conformation is 7 kJmol^{-1} lower than S…S conformation (Fig. S3), consistent with chalcogen (S…O)[26] and N…S interactions[28] reported previously.

Polymer Orientation and Hole Mobilities.

Polymer orientation in pristine and $PC_{61}BM$ blend films were characterized by two-dimensional grazing-incidence X-ray diffraction (2D-GIXRD) shown in Fig. 2. Thin spun-coat pristine films (ca. 60 nm) contained intense tail of direct X-ray overlapping the weak diffraction of polymer in the out-of-plane low angle diffraction region. This hampers the quantitative analysis of face-on and edge-on orientation (Fig. S4), and thus the thick pristine films (ca. 1 μm) prepared by drop-casting were evaluated. It needs to be mentioned, though, that the π-π stacking distance and face-on/edge-on orientations were mostly unchanged between spun-coat and drop-cast films. The blend films were prepared in the same way with the optimal OPV devices fabrication (vide infra). Surprisingly, all of the pristine polymers indicate profound face-on orientation with negligibly small edge-on peaks. The π-π stacking distances are moderate, ranging from 3.57 Å for **BT1** to 3.67 Å for **TT2** (Table 2). Although the π-π stacking distances did not display obvious variations by the molecular structure, the lamellar packing distances were rationally increased from mono-thiophene spacer (24.8 Å for both **TT1** and **BT1**) to bis-thiophene one (26.1 Å for **TT2** and 25.4 Å **BT2**).

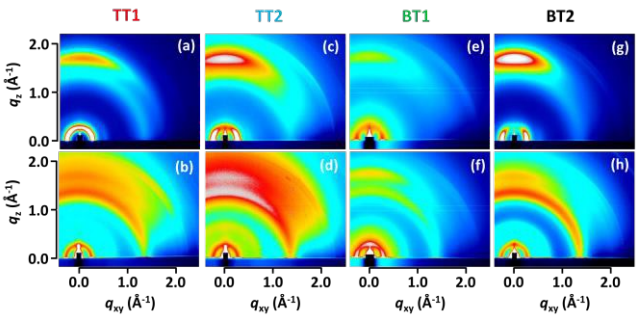

Fig. 2. 2D-GIXRD patterns of pristine **TT1** (a), **TT2** (c), **BT1** (e) and **BT2** (g) drop-cast on ITO substrate. (b) (d) (f) (h) are the patterns of optimal OPV devices (polymer and $PC_{61}BM$ blends).

The ratio of face-on orientation ($R_{face\text{-}on}$ in %) was evaluated by $I_{ip}/(I_{ip}+I_{op})$, where I_{ip} and I_{op} are the peak intensities of (100) diffraction in the in-plane and out-of-plane directions, respectively (Fig. S5). It should be noted that $R_{face\text{-}on}$ is an approximation of face-on fraction in XRD-active crystalline part,[17,29] and thus $R_{face\text{-}on}$ is not directly associated with crystallinity of polymer. Besides, out-of-plane diffraction tend to appear with higher intensity than its actual composition, due to the combination of the thin film geometry and the constraint of one axis to the sample plane in polar figure.[30] By taking these into account, $R_{face\text{-}on}$ evaluation in this study is supposed to be slightly underestimated, since the out-of-plane diffraction at the small scattering vector attributed to edge-on orientation could be stronger than is the actual case. As listed in Table 2, pristine **BT2** shows a pronounced $R_{face\text{-}on}$ as high as 95% (the ratio of face-on to edge-on, I_{ip}/I_{op} is ca. 19). To the best of our knowledge, this is the top-class preferential face-on orientation reported so far in OPV polymers. Examples of high $R_{face\text{-}on}$ polymer are thiazolothiazole (91%)[17] and dicarboximide-dithiophene (PBTI3T, 93%, face-on:edge-on = 14)[31] polymers. The pioneering LBPs of benzodithiophene (BDT)-thienopyrroledione (PBDTTPD)[32,33] and BDT-thienothiophene (PTB7 and PBDTTT-C-T)[34-36] of which PCE exceeded 6–7%

Table 2. 2D-GIXRD and SCLC Data of BTIDG Polymers

Film (p/n ratio)	π-π/Å[a]	IL/Å[b]	$R_{face\text{-}on}$[c]	$\mu_h/10^{-5}$ cm^{2}V^{-1}s^{-1}
TT1	3.64	24.8	67 %	1.0
TT1:$PC_{61}BM$ (1:1)	3.64	24.8	40 %	6.8
TT2	3.67	26.1	80 %	5.9
TT2:$PC_{61}BM$ (1:2)	3.71	26.1	73 %	10
BT1	3.57	24.8	93 %	0.18
BT1:$PC_{61}BM$ (1:2)	3.54	23.7	68 %	4.9
BT2	3.66	25.4	95 %	120
BT2:$PC_{61}BM$ (1:2)	3.64	24.8	75 %	12

[a] Calculated from the (010) peaks in the out-of-plane direction. [b] Interlamellar distance calculated from the (100) peaks in the in-plane direction. [c] Calculated by $I_{ip}/(I_{ip}+I_{op})$.

in 2010 also have highly face-on orientation. We extracted the $R_{face\text{-}on}$ of 94% for pristine PTB7 from its 2D-GIXRD image (Fig. S5),[37] corroborating the high face-on orientation of the successful polymer. Other early LBPs such as carbazole-benzothiaziazole (PCDTBT)[38] and cyclopentadithiophene-benzothiaziazole (PCPDTBT)[39] also indicate the face-on preferred 2D-GIXRD images along with rather amorphous features. Since the face-on orientation is advantageous for vertical charge transport in OPV cells,[13,17,31] recent development of high performance LBPs is directed to control of the polymer orientation as well as bandgap engineering. The second highest $R_{face\text{-}on}$ of 93% was found for **BT1**, which is followed by **TT2** (80%) and **TT1** (67%).

Due to the complicated factors affecting the polymer orientation, a rational molecular design of face-on polymer remains poorly understood. Solubility, shape of solubilizing alkyl chains (branched one is likely more favorable for face-on than linear one), and the length of alkyl chains have been supposed as the premiere factors that control polymer orientation. In the present study, the sizes of π-plane (BT >TT) and spacer (bithiophene:2 > thiophene:1) were found to have an impact on improving face-on orientation. In sharp contrast, mixing with $PC_{61}BM$ significantly decreased the face-on orientation. The similar trend appeared in all blend films, where $R_{face\text{-}on}$ dropped by 10–20 % (Table 2). For instance, the most face-on-preferred **BT2** indicate the $R_{face\text{-}on}$ of 75% in the PCBM blend, accompanying with a decrease of diffraction intensity.

Hole mobilities (μ_h) of BTIDG polymers and their blends with $PC_{61}BM$ were measured by space-charge limited current (SCLC) technique[40] (Table 2 and Fig. S6). Remarkably, the most face-on-orientated pristine **BT2** demonstrated the highest μ_h of 1.2×10^{-3} $cm^2V^{-1}s^{-1}$, while the other polymers gave 2–3 orders of magnitude smaller values (10^{-5}–10^{-6} $cm^2V^{-1}s^{-1}$). **BT2**:$PC_{61}BM$ blend film showed the μ_h of 1.2×10^{-4} $cm^2V^{-1}s^{-1}$ decreased by one order of magnitude; however, this is still higher than the other polymer blends (10^{-4}–10^{-5} $cm^2V^{-1}s^{-1}$). Despite the reduced diffraction intensities upon mixing with $PC_{61}BM$, the π-π stacking and lamellar packing distances were mostly unchanged, indicative of no intercalation into the polymer crystallites. Interestingly, μ_h of $PC_{61}BM$-blended **TT1**, **TT2**, and **BT1** are comparable to or even higher than those of pristine polymers, regardless of the deceased $R_{face\text{-}on}$. Although the cause of the enhanced μ_h in the blend films is unclear, this might merit the OPV performance which prefers a high μ_h in the vertical direction.

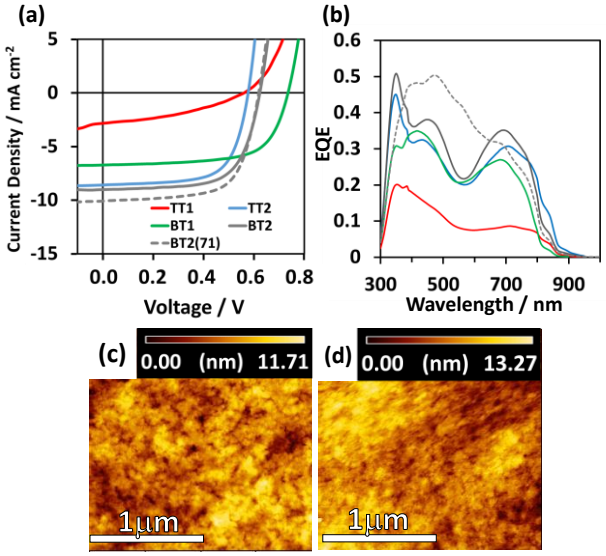

Fig. 3. (a) *J-V* curves and (b) EQE spectra of the best-performing OPV devices. AFM topology images (2 × 2 μm) of (c) **BT2**:$PC_{61}BM$ = 1:2 and (d) **BT2**:$PC_{71}BM$ = 1:2. The scale bar at the bottom is 1 μm.

Solar Cell Performance.

Fig. 3a shows current-voltage curves of normal cell OPV (PEDOT:PSS/active layer/Ca/Al). The active layers were prepared from chlorobenzene (CB) solution with 3 vol% solvent additive of either 1,8-diiodeoctane (DIO) or 1-chloronaphthalene (CN). We have examined the p/n blend ratio (1:1~1:5), film thickness, and thermal annealing effect (80, 120, and 150 ˚C). The optimal device parameters are summarized in Table 3, where the best blend ratio depends on the polymer (from 1:1 to 1:3) and no thermal annealing is preferred for all the polymers. The other low-performing device outputs are listed in Tables S1-S4. Except for the low PCE of **TT1** (0.60%), **TT2**, **BT1**, and **BT2** indicated the comparable PCEs from 3.3 to 3.7%. The best PCE of 3.74% (average 3.47%) was achieved for **BT2**:$PC_{61}BM$ = 1:2 with the open-circuit voltage (V_{oc}) of 0.62 V, J_{sc} of 10.07 mA cm^{-2}, and fill factor (FF) of 0.66. The external quantum efficiency (EQE) spectra of **TT2**, **BT1**, and **BT2** shown in Fig. 3b present almost identical features corresponding to the superposition of polymer and $PC_{61}BM$ absorption spectra. The calculated J_{sc} (= J_{sc}^{calc}) from the EQE spectra are in excellent agreement with J_{sc} under 1 sun (Table 3), indicative of the appropriate evaluation. The lowest-

Table 3. Summary of Optimized OPV Device Performances of BTIDG Polymers.

Blend[a]	p/n ratio[b]	*L* / nm [c]	PCE (average) / % [d]	V_{oc} / *V*	J_{sc} / mA cm^{-2}	FF	J_{sc}^{calc}/ mA cm^{-2} (J_{sc} / J_{sc}^{calc}) [e]
TT1:$PC_{61}BM$	1:1	79	0.60 (0.48)	0.56	2.83	0.38	2.85 (0.99)
TT2:$PC_{61}BM$	1:2	150	3.40 (3.22)	0.58	8.54	0.69	7.90 (1.08)
BT1:$PC_{61}BM$	1:3	84	3.29 (3.21)	0.73	6.72	0.67	6.74 (1.00)
BT2:$PC_{61}BM$	1:2	89	3.74 (3.47)	0.62	9.01	0.66	8.68 (1.04)
BT2:$PC_{71}BM$	1:2	90	4.18 (3.92)	0.62	10.07	0.67	10.04 (1.00)

[a] Normal cell structure (PEDOT:PSS/active layer/Ca/Al). The active layers were fabricated by chlorobenzene solution with 3 v/v % DIO or CN. No thermal annealing was applied for the active layer. [b] In weight % fraction. [c] Thickness of active layer. [d] The maximum PCE. The value in the brackets is an averaged PCE over at least 5 devices. [e] The calculated J_{sc} by integrating EQE spectrum. The value in the brackets is J_{sc} / J_{sc}^{calc}.

performing **TT1** shows a suppressed EQE spectrum and low J_{sc}, arisen from the lowest face-on orientation ($R_{face\text{-}on}$ = 40%) and molecular weight.

The film morphologies observed by atomic force microscopy (AFM) are almost similar (Figs. 3c and 3d and Fig. S7). V_{oc} are presumably proportional to the energy difference between HOMO of p-type polymer and LUMO of n-type fullerene with the energy loss ranging from 0.8 to 1.3 eV.[41] The highest V_{oc} of 0.73 V was obtained for **BT1** (HOMO = -5.50 eV), while those of other polymers having the almost same HOMO of -5.35– -5.43 eV were ca. 0.56–0.62 V, consistent with 0.1 V lower HOMOs.

To improve the PCE of the best-performing **BT2**-based OPV, $PC_{61}BM$ was replaced by $PC_{71}BM$ which has higher absorption in the visible region than the former. As a result, **BT2**:$PC_{71}BM$ boosted the PCE to 4.18% (average 3.92%), due to the increased J_{sc} of 10.1 mA cm^{-2} without sacrifices of V_{oc} (0.62 V) and FF (0.67). The film morphologies of **BT2**:$PC_{61}BM$ and **BT2**:$PC_{71}BM$ were almost identical as visualized in the AFM images of Figs. 3c and 3d. We also examined a thicker film of **BT2**:$PC_{61}BM$, because the updating high PCE of 9–10% was achieved for the thick active layers (ca. 300 nm) composed of crystalline polymer.[13,42,43] The PCE of 300 nm-thick **BT2**:$PC_{61}BM$ was 3.51%, being equal to the 120 nm-thick film (3.50%). Despite the identical V_{oc} (0.61 V), the J_{sc} and FF of the 300 nm-thick film were increased to 13.38 mA cm^{-2} and decreased to 0.43, respectively, indicative of the typical trade-off relationship.[17] On the manufacturing stage of OPV via high-throughput inkjet printing, a polymer without strong thickness dependence is highly favorable[44] in which **BT2** could be relevant to this criterion.

Conclusions

In conclusion, we designed and synthesized the new LBPs composed of asymmetric BTIDG acceptor and weak donors, affording suitable E_g^{opt} and HOMO levels. The 2D-GIXRD measurements revealed the polymer orientation is molecularly controlled by the size of donor π-plane and the number of alkylthiophene spacer, among which the top-class face-on orientation ($R_{face\text{-}on}$ = 95%) was demonstrated in pristine **BT2**. The best PCE of 4.2% was achieved in **BT2**:$PC_{71}BM$ without significant thickness dependence. Since the polymer:$PC_{71}BM$ films still suffer from a large decrease in face-on orientation by 10–20%, BTIDG-based polymers underpin further evolution of efficient OPV in which our work provides useful design guide on polymer face-on orientation.

Experimental

General. Steady-state photoabsorption spectroscopy was performed using a Jasco V-570 UV-vis spectrophotometer. Molecular weights of polymers were determined using the gel permeation chromatography (GPC) method with polystyrene standards. GPC analysis was performed with chloroform as an eluent at a flow rate of 1 cm^3 min^{-1} at 40 ˚C, on a SHIMADZU LC-20AT, CBM-20A, CTO-20A chromatography instrument connected to a SHIMADZU SPD-M20A UV-vis detector. PYS experiments were carried out by a Sumitomo Heavy Industry Co. PCR-202. GIXD experiments were conducted at the SPring-8 on the beam line BL19B2 or BL46XU using 12.39 keV (λ = 1 Å) X-ray. The GIXD patterns were recorded with a 2-D image detector (Pilatus 300K). AFM observations were performed by a Seiko Instruments Inc. model Nanocute OP and Nanonavi II**.**

Materials. The polymers were synthesized according to our previous reports[8] and following procedures. PCBM and solvents were purchased from Frontier Carbon Inc. and Kishida Chemical Inc., respectively, and used as received. All chemicals were purchased from Aldrich, Kanto Chemicals, Tokyo Chemical Inc. (TCI), or WAKO Chemical Co., and were used as received. Column chromatography was carried out on Silica Gel 60N (spherical, neutral) or NH silica gel from Fuji Silysia Chemical Ltd. Air- and water-sensitive synthetic steps were performed in a dried nitrogen or argon atmosphere using a standard Schlenk technique. All monomers were carefully purified prior to use in the polymerization.

Synthesis. Synthetic procedure of BTIDG molecules and polymers are shown in Scheme 1 and 2, respectively. The synthesis of precursors (5) and (7) is provided in the Electronic Supplementary Information.

6-bromo-1-(2-hexyldecyl)-3-[6-(2-hexyldecyl)-5-oxothieno[2,3-b]pyrrol-4-ylidene]indol-2-one(8). Compound (5) (127 mg, 0.34 mmol), compound (7) (140 mg, 0.32 mmol), acetic acid (2.6 mL) were added to 30 mL two-neck flask at room temperature under the atmosphere of nitrogen. The reaction solution was stirred at 100 ˚C for 15 h. After the reaction, the reaction mixture was quenched with water and extracted with hexane, and the solvent was removed under vacuum. The residue was purified by flash chromatography on neutral silica gel, eluted with hexane/ethylacetate (10/1). The product was obtained as purple oil (113.6 mg, 1.4×10^{-4} mol, yield: 44 %). ^{1}HNMR (400 MHz, $CDCl_3$), δ 0.85 (m, 12H), 1.24 – 1.32 (m, 48H), 1.84 (m, 2H), 3.64 (d, J = 7.6 Hz, 2H), 3.69 (d, J = 7.2 Hz, 2H), 6.74 (d, J = 5.6 Hz, 1H), 6.97 (d, J = 2.0 Hz, 1H), 7.23 (dd, J = 8.4, 2.0 Hz, 1H), 7.60 (d, J = 5.6 Hz, 1H), 8.4 (d, J = 8.4 Hz, 1H). Anal. calcd for $C_{46}H_{71}BrN_2O_2S$: C, 69.41; H, 8.99; Br, 10.04; N, 3.52; O, 4.02; S, 4.03. Found; C, 68.97; H, 9.12; Br, 10.58; N, 3.50; S, 4.14 %. MS (MALDI-TOF): m/z calcd for $C_{46}H_{71}BrN_2O_2S$: 795.04[M^+]; found: 796.16[M^+].

6-bromo-3-[2-bromo-6-(2-hexyldecyl)-5-oxothieno[2,3-b]pyrrol-4-ylidene]-1-(2-hexyldecyl)indol-2-one(9). Compound (8) (0.46 g, 5.8×10^{-4} mol), N-bromosuccinimide (NBS) (0.10 g, 5.9×10^{-4} mol), dry tetrahydrofuran (THF) (9.7 mL) were added to dried 50 mL flask. After stirring 12 h at room temperature under the atmosphere of nitrogen, the reaction mixture was quenched with H_2O and extracted with Hexane. The solvent was removed under vacuum, and the residue was purified by flash chromatography on neutral silica gel, eluted with hexane/ethylacetate (15/1). The product was obtained as purple oil (0.48 g, 5.5×10^{-4} mol, yield: 95 %). ^{1}HNMR (400 MHz, $CDCl_3$), δ 0.86 (m, 12H), 1.24 – 1.29 (m, 48H), 1.84 (m, 2H), 3.57 (d, J = 7.2 Hz, 2H), 3.64 (d, J = 7.6 Hz, 2H), 6.74 (s, 1H), 6.91 (d, J = 2.0 Hz, 1H), 7.17 (dd, J = 8.4, 2.0 Hz, 1H) , 9.07 (d, J = 8.4 Hz, 1H). Anal. calcd for $C_{46}H_{70}Br_2N_2O_2S$: C, 63.15; H, 8.06; Br, 18.27; N, 3.20; O, 3.66; S, 3.66. Found; C, 63.29; H, 8.09; Br, 18.12; N, 3.18; S, 3.76 %. MS (MALDI-TOF): m/z calcd for $C_{46}H_{70}Br_2N_2O_2S$: 873.93[M^+]; found: 874.07[M^+].

1-(2-hexyldecyl)-3-[6-(2-hexyldecyl)-5-oxo-2-(thiophen-3-yl)thieno[2,3-b]pyrrol-4-lidene]-6-(thiophen-2-yl)indol-2-one(10). Compound (9) (0.094 g, 1.1 × 10^{-4} mol), 2-Trimethylstannyl-4-bromothiophene (18) (0.089 g, 2.1 × 10^{-4} mol), xylene (1.5 mL), $Pd(PPh_3)_4$ (6.2 mg, 5.4 × 10^{-6} mol) were added to dried 20 mL Schlenk flask under nitrogen atmosphere. After refluxing at 150 ˚C for 5 h, the reaction mixture was diluted by Dichloromethane and filtered with Celite. It was purified by flash chromatography on neutral silica gel, eluted with hexane/ethylacetate (20/1). The product was obtained as purple oil (0.113 g, 9.3 × 10^{-5} mol, yield: 86 %). ^{1}HNMR (400 MHz, $CDCl_3$), δ 0.86 (m, 18H), 1.24-1.37 (m, 98H), 1.65 (m, 4H), 1.84 (m, 2H), 3.66 (d, *J* = 6.8 Hz, 2H), 3.77 (d, *J* = 6.4 Hz, 2H), 6.78 (s, 1H), 6.93 (d, *J* = 2.0 Hz, 1H), 7.04 (d, *J* = 1.6 Hz, 1H), 7.30 (d, *J* = 1.2 Hz, 1H), 7.33 (d, *J* = 1.6 Hz, 1H), 9.20 (d, *J* = 8.4 Hz, 1H).

6-(5-bromothiophen-2-yl)-3-[2-(5-bromothiophen-3-yl)-6-(2-hexyldecyl)-5-oxothieno[2,3-b]pyrrol-4-ylidene]-1-(2-hexyldecyl)indol-2-one(11). Compound (10) (0.12 g, 9.3 × 10^{-5} mol), NBS (0.035 g, 2.0 × 10^{-4} mol), THF (1.5 mL) were added to 30 mL two neck flask, and the reaction mixture was stirred for 4 h at room temperature. The blue solution was quenched with H_2O, and the solvent was removed after the extraction with ethylacetate. The residue was purified by flash chromatography with neutral silica gel, eluted with hexane/ethylacetate (50/1) the product was obtained as blue purple oil (0.12 g, 8.7 × 10^{-5} mol, yield: 91 %). ^{1}HNMR (400 MHz, $CDCl_3$), δ 0.88 (m, 18H), 1.24 (m, 98H), 1.62 (m, 4H), 1.83 (m, 2H), 3.53 (d, *J* = 7.2 Hz, 2H), 3.64 (d, *J* = 6.4 Hz, 2H), 6.52 (s, 1H), 6.77 (s, 1H), 7.01 (s, 1H), 7.09 (s, 1H), 7.14 (dd, *J* = 8.0, 1.6 Hz, 1H), 9.07 (d, *J* = 8.4 Hz, 1H).

General procedure of synthesis of the copolymers. The synthetic route for copolymers (TT1, TT2, BT1, and BT2) is shown in Scheme 2. The specific condition of each copolymer is given in Electronic Supplementary Information. Polymerization steps for BTIDG polymers were carried out through the palladium(0)-catalyzed Stille cross-coupling reactions. For Stille cross-coupling reaction, 1 equiv. of dibromo monomers and 1 equiv. of bistrimethylstannyl monomers were added into anhydrous xylene in a 20 mL Schlenk flask. Tetrakis- (triphenylphosphine)palladium(0) (0.05 eqiv.) was transferred into the mixture in a nitrogen atmosphere. The reaction mixture was stirred at 150 ˚C for 1-2 h, and then an excess amount of bromobenzene and trimethyltin benzene were added to end-cap the trimethylstannyl and bromo groups for 30 min, respectively. After adding a four-fold larger amount of xylene than the reaction solution, the reaction mixture was cooled to 40 ˚C and added slowly into a vigorously stirred ten-fold larger volume of methanol than the diluted reaction mixture. The polymers were collected by filtration and dried under vacuum. The dried crude polymers were dissolved in $CHCl_3$ (200 mL) and further purified by column chromatography on neutral silica gel and six layered interleave NH silica with a NH_2 silica gel layer to remove the metallic impurities. The obtained $CHCl_3$ solution was filtered through celite and the solvent was removed under vacuum. The remaining solid was dissolved in a minimum amount of $CHCl_3$ and reprecipitated by six-fold larger amount of acetone than dissolved solution to remove oligomers. The precipitate was filtered using a membrane filter and dried under vacuum.

Organic photovoltaic cell (OPV). The main paragraph text follows directly on here. The procedures of fabrication of OPV followed the reference.[45] A PEDOT:PSS (Heraeus Clevios P VP AI 4083) layer was cast onto the cleaned ITO layer by spin-coating after passing through a 0.2 μm filter. The substrate was annealed on a hot plate at 120 °C for 30 min. An active layer consisting of polymer and PCBM (purchased from Frontier Carbon Inc.) was cast on top of the PEDOT:PSS buffer layer in a nitrogen glove box by spin-coating after passing through a 0.2 μm filter. The thickness was around 80–90 nm for **TT1**, **BT1**, and **BT2**, and 150 nm for **TT2**. No thermal annealing was applied. Solvent and solvent additive were completely removed in a vacuum chamber by keeping the device for at least 30 min. A cathode consisting of 20 nm Ca and 100 nm Al layers was sequentially deposited through a shadow mask on top of the active layers by thermal evaporation in a vacuum chamber. The resulting device configuration was ITO (120–160 nm)/PEDOT:PSS (45–60 nm)/ active layer/Ca (20 nm)/Al (100 nm) with an active area of 7.1 mm^2. Current-Voltage curves were measured using a source-measure unit (ADCMT Corp., 6241A) under AM 1.5 G solar illumination at 100 mW cm^{-2} (1 sun, monitored by a calibrated standard cell, Bunko Keiki SM-250KD) from a 300 W solar simulator (SAN-EI Corp., XES-301S). The EQE spectra were measured by a Bunko Keiki model BS-520BK equipped with a Keithley model 2401 source meter. The monochromated light power was calibrated by a silicon photovoltaic cell, Bunko Keiki model S1337-1010BQ.

Space-Charge Limited Current (SCLC). ITO coated glass substrates were subsequently cleaned in detergent, distilled water, acetone and isopropanol for 10 min each ultrasonication. Aluminum was vapor deposited on the ITO surface with patterned mask as guide electrode. The substrates were further UV-ozone treated and a layer of PEDOT:PSS (Heraeus Clevios P VP AI 4083) was spincoated after passing through a 0.2 mm filter. They were annealed on a hot plate at 120 ˚C for 10 min, and then inserted into a glove box filled with nitrogen. A solution of polymer in chlorobenzene was heated at 80 ˚C under stirring for at least 2 h to dissolve polymer completely. A thin layer of BTIDG polymer or polymer:PCBM blend was spin-coated from the polymer solution or solution of the OPV best-performing blend ratio, respectively. A gold layer with 70-100 nm in thick was deposited by thermal evaporation in a vacuum chamber. The current-voltage (*J*-*V*) curves were measured using an ADCMT Corp. 6241A source meter. The hole mobility was determined by fitting the *J*-*V* curve into the Mott-Gurney law, $J = 9\varepsilon_r\varepsilon_0\mu (V\text{-}V_{bi})^2/(8L^3)$, where ε_0 is the permittivity of free space, ε_r is the relative dielectric constant of the material, μ is the hole (or electron) mobility, *V* is the voltage, V_{bi} is the built-in voltage, and *L* is the layer thickness.[46]

Acknowledgements

This work was supported by KAKENHI grants from the Ministry of Education, Culture, Sports, Science and Technology (MEXT) of Japan (No. 26102011 and 25288084). M. I. acknowledges the financial support of a JSPS scholarship (No. 261480). The authors appreciate Dr. Keisuke Tajima at RIKEN, Japan for providing 2D-GIXRD data of pristine PTB7 film[37] and Dr. Itaru Osaka at RIKEN, Japan for 2D-GIXRD experiments at SPring8 (proposal 2013B1719).

References

1 L. Dou, J. You, Z. Hong, Z. Xu, G. Li, R. A. Street, Y. Yang, *Adv. Mater*. **2013**, *25*, 6642−6671.
2 J. E. Coughlin, Z. B. Henson, G. C. Welch, G. C. Bazan, *Acc. Chem. Res.* **2014**, *47*, 257−270.
3 S. D. Dimitrov, J. R. Durrant, *Chem. Mater*. **2014**, *26*, 616−630.
4 J. H. Kim, C. E. Song, B. S. Kim, I. N. Kang, W. S. Shin, D. H. Hwang, *Chem. Mater.* **2014**, *26*, 1234−1242.
5 T. Lei, J. –Y. Wang, J. Pei, *Chem. Mater.* **2014**, 26, 594−603.
6 R. Stalder, J. Mei, K. R. Graham, L. A. Estrada, J. R. Reynolds, *Chem. Mater.* **2014**, 26, 664–678.
7 C.- C. Ho, C. A-. Chen, C. –Y. Chang, S. B. Darling, W. –F. Su, *J. Mater. Chem. A*. **2014**, *2*, 8026–8032.
8 Y. Koizumi, M. Ide, A. Saeki, C. Vijayakumar, B. Balan, M. Kawamoto, S. Seki, *Polym. Chem*. **2013**, *4*, 484-494.
9 R. S. Ashraf, A. J. Kronemeijer, D. I. James, H. Sirringhaus, I. McCulloch, *Chem. Commun*. **2012**, *48*, 3939−3941.
10 G. W. P. Van Pruissen, F. Gholamrezaie, M. M. Wienk, R. A. J. Janssen, *J. Mater. Chem.* **2012**, *22*, 20387−20393.
11 M. Ide, Y. Koizumi, A. Saeki, Y. Izumiya, H. Ohkita, S. Ito, S. Seki, *J. Phys. Chem. C*, **2013**, *117*, 26859−26870.
12 M. S. Chen, J. R. Niskala, D. A. Unruh, C. K. Chu, O. P. Lee, J. M. J. Fréchet, *Chem. Mater*., **2013**, *25*, 4088–4096.
13 V. Vohra, K. Kawashima, T. Kakara, T. Koganezawa, I. Osaka, K. Takimiya, H. Murata, *Nat. Photo.* **2015**, 9, 403-409.
14 G. Ren, C. W. Schlenker, E. Ahmed, S. Subramaniyan, S. Olthof, A. Kahn, D. S. Ginger, S. A. Jenekhe, *Adv. Funct. Mater*. **2013**, *23*, 1238–1249.
15 A. Bhuwalka, J. F. Mike, M. He, J. J Intemann, T. Nelson, M. D. Ewan, R. A. Roggers, Z. Lin, M. Jeffries-EL, *Macromolecules*, **2011**, *44*, 9611–9617.
16 S. Subramaniyan, H. Xin, F. S. Kim, S. Shoaee, J. R. Durrant, S. A. Jenekhe, *Adv. Energy Mater*. **2011**, *1*, 854–860.
17 I. Osaka, M. Saito, T. Koganezawa, K. Takimiya, *Adv. Mater*. **2014**, *26*, 331–338.
18 M. Tsuji, A. Saeki, Y. Koizumi, N. Matsuyama, C. Vijayakumar, S. Seki, *Adv. Funct. Mater*. **2014**, *24*, 28–36.
19 A. Saeki, M. Tsuji, S. Yoshikawa, A. Gopal, S. Seki, *J. Mater. Chem. A*, **2014**, *2*, 6075–6080.
20 A. Gopal, A. Saeki, M. Ide, S. Seki, *ACS Sustainable Chem. Eng*. **2014**, *2*, 2613–2622.
21 D. Veldman, S. C. J. Meskers, R. A. J. Janssen, *Adv. Funct. Mater*. **2009**, *19*, 1939–1948.
22 B. W. Larson, J. B. Whitaker, X. –B. Wang, A. A. Popov, G. Rumbles, N. Kopidakis, S. H. Strauss, O. V. Boltalina, *J. Phys. Chem. C* **2013**, *117*, 14958−14964.
23 M. C. Scharber, D. Mühlbacher, M. Koppe, P. Denk, C. Waldauf, A. J. Heeger, C. J. Brabec, *Adv. Mater*. **2006**, *18*, 789−794.
24 Y. Shin, X. Lin, *J. Phys. Chem. C* **2013**, *117*, 12432−12437.
25 T. Lei, Y. Cao, X. Zhou, Y. Peng, J. Bian, J. Pei, *Chem. Mater*. **2012**, *24*, 1762−1770.
26 G. K. Dutta, A-R. Han, J. Lee, Y. Kim, J. H. Oh, C. Yang, *Adv. Funct. Mater*. **2013**, *23*, 5317–5325.
27 G. Kim, S.-J. Kang, G. K. Dutta, Y. –K. Han, T. J. Shin, Y. Y. Noh, C. Yang, *J. Am. Chem. Soc*. **2014**, *136*, 9477−9483.
28 H. Bronstein, M. Hurhangee, E. C. Fregoso, D. Beatrup, Y. W. Soon, Z. Huang, A. Hadipour, P. S. Tuladhar, S. Rossbauer, E.-H. Sohn, S. Shoaee, S. D. Dimitrov, J. M. Frost, R. S. Ashraf, T. Kirchartz, S. E. Watkins, K. Song, T. Anthopoulos, J. Nelson, B. P. Rand, J. R. Durrant, I. McCulloch, *Chem. Mater.* **2013**, *25*, 4239−4249.
29 J. Rivnay, S. C. B. Mannsfeld, C. E. Miller, A. Salleo, M. F. Toney, *Chem. Rev*. **2012**, *112*, 5488−5519.
30 D. M. DeLongchamp, R. J. Kline, A. Herzing, *Energy Environ. Sci*. **2012**, *5*, 5980-5993.
31 X. Guo, N. Zhou, S. J. Lou, J. Smith, D. B. Tice, J. W. Hennek, R. P. Ortiz, J. T. L. Navarrete, S. Li, J. Strzalka, L. X. Chen, R. P. H. Chang, A. Facchetti, T. J. Marks, *Nature Photo*. **2013**, *7*, 825–833.
32 C. Piliego, T. W. Holcombe, J. D. Douglas, C. H. Woo, P. M. Beaujuge, J. M. J. Fréchet, *J. Am. Chem. Soc*. **2010**, *132*, 7595−7597.
33 Y. Zou, A. Najari, P. Berrouard, S. Beaupré, B. R. Aïch, Y. Tao, M. Leclerc, *J. Am. Chem. Soc*. **2010**, *132*, 5330−5331.
34 Y. Liang, Z. Xu, J. Xia, S.-T. Tsai, Y. Wu, G. Li, C. Ray, L. Yu, *Adv. Mater*. **2010**, *22*, E135−E138.
35 H. –Y. Chen, J. Hou, S. Zhang, Y. Liang, G. Yang, Y. Yang, L. Yu, Y. Wu, G. Li, *Nature Photo*. **2009**, *3*, 649−653.
36 M. Shao, J. K. Keum, R. Kumar, J. Chen, J. F. Browning, S. Das, W. Chen, J. Hou, C. Do, K. C. Littrell, A. Rondinone, D. B. Geohegan, B. G. Sumpter, K. Xiao, *Adv. Funct. Mater*. **2014**, *24*, 6647–6657.
37 E. Zhou, M. Nakano, S. Izawa, J. Cong, I. Osaka, K. Takimiya, K. Tajima, *ACS Macro Lett*. **2014**, *3*, 872−875.
38 Z. M. Beiley, E. T. Hoke, R. Noriega, J. Dacuña, G. F. Burkhard, J. A. Bartelt, A. Salleo, M. F. Toney, M. D. McGehee, *Adv. Energy Mater*. **2011**, *1*, 954–962.
39 A. A. Y. Guilbert, J. M. Frost, T. Agostinelli, E. Pires, S. Lilliu, J. E. Macdonald, J. Nelson, *Chem. Mater*. **2014**, *26*, 1226−1233.
40 P. W. M. Blom, M. J. M. de Jong, J. J. M. Vleggaar, *Appl. Phys. Lett*. **1996**, *68*, 3308–3310.
41 M. A. Faist, T. Kirchartz, W. Gong, R. S. Ashraf, I. McCulloch, J. C. de Mello, N. J. Ekins-Daukes, D. D. C. Bradley, J. Nelson, J. *J. Am. Chem. Soc*. **2012**, *134*, 685−692.
42 Y. Liu, J. Zhao, Z. Li, C. Mu, W. Ma, H. Hu, K. Jiang, H. Lin, H. Ade, H. Yan, *Nature Commun*. **2014**, *5*, 5293/1−8.
43 T. L. Nguyen, H. Choi, S.-J. Ko, M. A. Uddin, B. Walker, S. Yum, J.-E. Jeong, M. H. Yun, T. J. Shin, S. Hwang, J. Y. Kim, H. Y. Woo, *Energy Environ. Sci*. **2014**, *7*, 3040−3051.
44 R. Søndergaard, M. Hösel, D. Angmo, T. T. Larsen-Olsen, F. C. Krebs, *Mater. Today* **2012**, *15*, 36−49.
45 A. Saeki, M. Tsuji, S. Seki, S. *Adv. Energy Mater.* **2011**, *1*, 661–669.
46 C. Melzer, E. J. Koop, V. D. Mihailetchi, P. W. M. Blom, *Adv. Funct. Mater.* **2004**, *14*, 865–870.

TOC